

Article

Influence of NaCl Freeze–Thaw Cycles on the Mechanical Strength of Reactive Powder Concrete with the Assembly Unit of Sulphoaluminate Cement and Ordinary Portland Cement

Zhangjie Cai ¹ and Hui Wang ^{2,3,*}

¹ Civil Engineering Department, Yancheng Institute of Technology, Yancheng 224051, China; caizhangjie@aliyun.com

² School of Civil and Environmental Engineering, Ningbo University, Ningbo 315000, China

³ State Key Laboratory of Materials-Oriented Chemical Engineering, Nanjing University of Technology, Nanjing 210000, China

* Correspondence: huiwang123@aliyun.com

Abstract: The influence of sulphoaluminate cement and the dosage of polypropylene fibers on the basic mechanical strengths (compressive and flexural strengths) of reactive powder concrete (RPC) cured for 1 d, 3 d, 7 d, 14 d and 28 d is studied in this research. The content of sulphoaluminate cement ranges from 0% to 100% and the dosages of polypropylene fibers are 0%~3.5%, respectively. Moreover, the mechanical properties (compressive and flexural strengths), the relative dynamic elastic modulus (*RDEM*) and the chloride permeability of specimens with 50% sulphoaluminate cement and different dosages of polypropylene fibers are determined after the specimens are exposed to different NaCl freeze–thaw cycles. The water–binder ratio in this study is 0.25, and the sand-to-binder ratio is 1.25. Results show that the relationship between the mechanical strengths of RPC at early curing ages (lower than 7 d) and the sulphoaluminate cement content is a linear function with a positive correlation. However, when the curing age reaches 14 d, the compressive and flexural strengths decrease in the form of a linear function with the addition of sulphoaluminate cement. The correlation between the mechanical strengths and polypropylene fiber volume is a positive quadratic function. However, the mass loss rate and flexural strength loss rate increased in the form of a quadratic function, and *RDEM* shows a negative quadratic function with the freeze–thaw cycles. Moreover, the compressive strength loss rate increases linearly with the freeze–thaw cycle. The addition of polypropylene fibers can effectively improve the freeze–thaw resistance of cement mortar with an assembly unit of ordinary cement and sulphoaluminate cement.

Keywords: sulphoaluminate cement; polypropylene fibers; reactive powder concrete; relative dynamic elastic modulus; NaCl freeze–thaw cycles



Citation: Cai, Z.; Wang, H. Influence of NaCl Freeze–Thaw Cycles on the Mechanical Strength of Reactive Powder Concrete with the Assembly Unit of Sulphoaluminate Cement and Ordinary Portland Cement. *Coatings* **2021**, *11*, 1238. <https://doi.org/10.3390/coatings11101238>

Academic Editors: Andrea Nobili and Valeria Vignali

Received: 13 July 2021

Accepted: 1 October 2021

Published: 12 October 2021

Publisher's Note: MDPI stays neutral with regard to jurisdictional claims in published maps and institutional affiliations.



Copyright: © 2021 by the authors. Licensee MDPI, Basel, Switzerland. This article is an open access article distributed under the terms and conditions of the Creative Commons Attribution (CC BY) license (<https://creativecommons.org/licenses/by/4.0/>).

1. Introduction

Nowadays, large-scale marine concrete constructs (like Hangzhou Bay Bridge, Jiaozhou Bay Bridge, and Hong Kong-Zhuhai-Macao Bridge etc.) have been widely used in China's civil engineering construction projects. However, when the concrete structure has been put to use in a coastal environment over a long period, the concrete materials can be seriously damaged due to the complex chloride corrosion from seawater [1]. In order to solve these problems, the damaged concrete structures need to be repaired routinely. Additionally, some important traffic structures in coastal cities, such as sea crossing bridges and highways, are frequently damaged due to the marine environment. The damages to concrete construction should be repaired quickly so as to prevent further deterioration, traffic jams and other problems [2]. In response to these problems, fast-hardening, high-performance, cement-based materials are needed.

Conventional pavement repairing materials cannot be put into use until they have been cured for more than 3 days. Therefore, the traffic cannot pass until the strength reaches

a higher value. Sulphoaluminate cement is a kind of cement with a fast setting speed which has been used as a kind of rapid repairing material for several years. Additionally, a smaller amount of carbon dioxide is produced during the productive process of sulphoaluminate cement [3]. Some researchers [4] have found that the flexural and compressive strengths of sulphoaluminate cement-based materials with a dosage of steel fibers higher than or equal to 1.5% are higher than 17 MPa and 37.5 MPa, respectively, after curing for 5 h. It can be summarized from some studies that sulphoaluminate cement-based materials possess high early strength (cured for less than 1 day). However, the mechanical strength is lower than that of Portland cement-based materials, and the cost of sulphoaluminate cement-based material is very high [5]. Therefore, it is necessary to decrease the manufacturing cost of rapid repairing cement-based materials. However, little attention to this has been reported. The use of the assembly unit of ordinary Portland cement and sulphoaluminate cement mixed with an early strength agent on rapid repairing cement-based materials could prove a good idea.

Ultra-high performance concrete (UHPC) with high strength and durability was first invented by an Aalborg cement researcher (Bache) in the 1980s. Reactive powder concrete (RPC) is a kind of ultra-high performance concrete which was first invented by the Bouygues Company in the 1990s. RPC is produced according to the maximum density theory. Due to high compactness, RPC shows excellent mechanical strength and durability. As pointed out by some researchers [6–9], the addition of carbon nanofibers and stainless steel fibers can improve the mechanical strength and the functional properties of RPC. Additionally, RPC reinforced with stainless steel fibers performs with excellent durability when the specimens are exposed to NaCl freeze–thaw cycles and NaCl dry–wet alternations [10]. Although, RPC with carbon nanofibers and stainless steel fibers shows excellent properties, the cost of the two kinds of fibers is expensive [11–13]. On the other hand, while the mechanical and durable performances of RPC have been investigated for many years, little attention has been paid to the mechanical properties and durability of RPC manufactured by the assembly unit of sulphoaluminate cement and ordinary Portland cement.

Polypropylene fiber is a kind of flexible fiber which has been applied in cement concrete for several years. This kind of fiber can effectively improve the mechanical strength of cement-based materials. Unlike steel fibers, polypropylene fibers may exhibit good corrosion resistance to chloride environments. Moreover, polypropylene fibers show better dispersion than basalt fibers and carbon fibers in a cement matrix. Therefore, this kind of fiber is suited to act as reinforcement fibers for cement concrete applied in marine environments [14,15]. The addition of sulphoaluminate cement can increase the mechanical and durable properties of RPC at an early curing age. Yet, the mechanical and durable properties may decay at late curing ages. The RPC manufactured by the assembly unit of sulphoaluminate cement and ordinary Portland cement may overcome this difficulty [16,17]. However, little research about RPC with the assembly unit of sulphoaluminate cement and ordinary Portland cement reinforced with polypropylene fibers has been reported.

In this study, the influence of sulphoaluminate cement and polypropylene fibers on the mechanical strengths (flexural strength and compressive strength) of RPC is studied. Moreover, the mechanical strengths and chloride ion permeability of polypropylene fibers and RPC mixed with the assembly unit of sulphoaluminate cement (SAC) and ordinary Portland cement are researched. This research study could provide a new kind of rapid repairing cement-based material in the future.

2. Experimental Materials and Methods

2.1. Raw Materials

Polypropylene fibers (PPFs) showing a density of 0.91 g/cm³, length of 10–13 mm, diameter of 18–48 µm and aspect ratio of 208–722 supplied by Hongyu Engineering Materials COBIT Co., Ltd., Jinan, China, were used in this study. The polypropylene fibers

presented a tensile strength of 710 MPa, and the average elastic modulus of polypropylene fibers is higher than 3850 MPa. This type of fiber possesses excellent acid and alkali resistance. Rapid hardening sulphoaluminate cement (RSAC; manufactured by Tangshan Polar Bear Building Materials Co., Ltd., Tangshan, China) and ordinary Portland cement (produced by Zhejiang Ningbo conch Co., Ltd. Ningbo, China), whose strength grade is 42.5 MPa, were applied in this study. Silica fume (SF) with a specific surface area of 15 m²/g, density of 2.2 g/cm³ and more than 98% SiO₂ was used in this study. Granulated blast furnace slag powder (GGBS) possessing a density of 2.9 g/cm³, a specific surface area of 436 m²/g and a loss on ignition of 2.3% was used as another cementitious material which can increase the activity of cement. The particle size distribution and the chemical composition of the cementitious materials are presented in Tables 1 and 2, respectively. The silica fume and granulated blast furnace slag powder were produced by Lingshou Aihong mineral products Co., Ltd., Lingshou, China. Lithium sulfate and calcium formate with a purity of higher than 99.9% produced by Yingshan New Material Technology Co., Ltd., Shanghai China, are used as early strength agents in the sulphoaluminate cement and ordinary Portland cement, respectively. Tartaric acid with higher than 99.9% purity and polycarboxylate superplasticizer with a 40% water reduction rate provided by Yingshan New Material Technology Co., Ltd. (Shanghai, China) were used to adjust the setting time of concrete. The quartz sand provided by Lingshou Aihong mineral products Co., Ltd., Lingshou, China with three sieving sizes of 1–0.71 mm, 0.59–0.35 mm and 0.15–0.297 mm are used as aggregate in this study. The mass ratio of the three sieving sizes is 1:1.5:0.8. In this study, the composition of the quartz sand is 99.6% SiO₂, 0.02% Fe₂O₃ and other ingredients. The binder–sand ratio of the RPC in this study is 1.25. The SAC contents in this study are 0%, 25%, 50%, 75% and 100%. While the content of SAC is 50%, the dosages of polypropylene fibers are 0%, 0.5%, 1.0%, 1.5%, 2.0%, 2.5%, 3.0% and 3.5% by volume of sulphoaluminate cement reactive powder concrete (SAC-RPC). For all specimens, the lithium sulfate and calcium formate in this study are 0.15% and 0.7% by mass of cementitious materials, respectively. The binder–water ratio in the mix proportions of SAC-RPC is 0.2. Table 3 shows the mix proportions of SAC-RPC. To manufacture RPC with the assembly unit of sulphoaluminate cement and Portland cement, the following steps should be carried out:

Firstly, all powder admixtures including sulphoaluminate cement, ordinary Portland cement (OPC), silica fume (SF), ground granulated blast furnace slag (GGBS) and quartz sand are first mixed in UJZ-15 mortar mixer Hebei Daoneng Construction Engineering Co., Ltd., Cangzhou, China, for 30 s, then polypropylene fiber is added and mixed for another 120 s. Finally, the water reducing agent is added and stirred into the mixture for the last 5.5 min. The slump flow of fresh RPC paste is adjusted to 210–230 mm by the water-reducing agent. DF-04 polyether surfactant with a density of 0.4 g/cm³ and a pH of 7.0–7.5 produced by Yingshan New Material Technology Co., Ltd. (Shanghai, China) is used to eliminate air bubbles in the RPC. The mechanical strengths of specimens with a size of 40 mm × 40 mm × 160 mm are determined after they have been cured in a standard curing environment (temperature of 20 ± 2 °C and relative humidity of above 95%) for 1 d, 3 d, 7 d, 14 d and 28 d, respectively. In the NaCl experiment, the mechanical strengths loss and the chloride migration coefficient (CMC) are determined with the specimens of size 40 mm × 40 mm × 160 mm and Φ100 mm × 50 mm, and specimens with dimensions of 100 mm × 100 mm × 400 mm were used for experiments on mass loss and relative dynamic modulus of elasticity during freeze–thaw cycles. Three specimens were prepared for each experiment. Prior to the experiments, all specimens were cured in a standard curing environment for 24 days. Finally, all specimens were immersed in a 3% NaCl solution for 4 d prior to the freeze–thaw cycle after curing for 24 d.

Table 1. Particle passing percentage of the cementitious materials/%.

Types	Particle Size/ μm						
	0.3	0.6	1	4	8	64	360
SAC	0	0.35	1.92	16.35	30.12	95.15	100
P·O cement	0	0.33	2.66	15.01	28.77	93.59	100
Slag power	0.025	0.1	3.51	19.63	35.01	97.9	100
Silica fume	31.2	58.3	82.3	100	100	100	100

Table 2. Chemical composition of the cementitious materials/%.

Types	SiO ₂	Al ₂ O ₃	Fe ₂ O ₃	MgO	CaO	SO ₃	Ti ₂ O
SAC	13.95	22.46	2.67	2.92	39.39	14.34	1.66
P·O cement	20.86	5.47	3.94	1.73	62.23	2.66	/
Slag power	34.06	14.74	0.23	9.73	35.93	0.23	3.51
Silica fume	90	0.2	0.6	0.2	0.4	0	7.4

Table 3. Mix proportions of SAC-RPC per one cubic meter (kg).

Water	OPC	SAC	SF	GGBS	Quartz Sand	Water-Reducer	PPFs	Li ₂ SO ₄	Tartaric Acid	Calcium Formate
244.4	740.7	0	370.3	111.1	977.9	16.3	0	0	0	5.2
244.4	555.5	185.2	370.3	111.1	977.9	16.3	0	1.3	0.3	3.9
244.4	370.4	370.4	370.3	111.1	977.9	16.3	0	2.6	0.6	2.6
244.4	185.2	555.5	370.3	111.1	977.9	16.3	0	3.9	0.8	1.3
244.4	0	740.7	370.3	111.1	977.9	16.3	0	5.2	1.1	0
244.4	370.4	370.4	370.3	111.1	977.9	16.3	0	2.6	0.6	2.6
244.4	370.4	370.4	370.3	111.1	977.9	16.3	0.46	2.6	0.6	2.6
244.4	370.4	370.4	370.3	111.1	977.9	16.3	0.91	2.6	0.6	2.6
244.4	370.4	370.4	370.3	111.1	977.9	16.3	1.37	2.6	0.6	2.6
244.4	370.4	370.4	370.3	111.1	977.9	16.3	1.82	2.6	0.6	2.6
244.4	370.4	370.4	370.3	111.1	977.9	16.3	2.28	2.6	0.6	2.6
244.4	370.4	370.4	370.3	111.1	977.9	16.3	2.73	2.6	0.6	2.6
244.4	370.4	370.4	370.3	111.1	977.9	16.3	3.19	2.6	0.6	2.6

2.2. Measurement Methods

The YAW-300 microcomputer full-automatic universal tester with the maximum testing force of 300 kN manufactured by Henruijin Co., Ltd., Jinan, China was used to measure the mechanical strengths of the RPC according to the GB/T 17671-1999 Chinese standard [18]. A rapid freeze–thaw concrete testing machine with temperatures ranging from $-15\text{ }^{\circ}\text{C}$ to $8\text{ }^{\circ}\text{C}$ was utilized for the NaCl freeze–thaw experiment according to the Chinese Standard GB/T 50082-2009 [19]. Before freeze–thaw cycles, each specimen was placed in a stainless steel sealed casing filled with 3% NaCl solution. The mechanical strengths (flexural and compressive strengths), the mass and the CMC were determined after 0, 50, 100, 150, 200, 250 and 300 freeze–thaw cycles. The mechanical strengths loss and the mass loss were calculated. The CMC experiment after different NaCl freeze–thaw cycles is described as follows: First, the NaCl solution on the surface of the cylinders ($\Phi 100\text{ mm} \times 50\text{ mm}$) was wiped out, and then the specimens were immersed in 3% NaCl solution in the concrete intelligent vacuum water saturator vacuum desiccator for the 3% NaCl solution treatment. After that, the sides of the treated specimen are sealed by silica gel. Finally, the specimens were settled in the chloride ion diffusion coefficient tester. The DT-20 dynamic elastic modulus tester produced by Cangzhou Huaheng Test Instrument Co., Ltd., Cangzhou, China was used to determine the relative dynamic modulus of the elasticity of SAC-RPC. The water or NaCl solution was wiped off with a wrung wet cloth. The test frequency

of the experiment ranges from 100 to 20,000 Hz. Figure 1 shows the testing process of the relative dynamic modulus of elasticity. The details for these experiments refer to the Chinese Standard GB/T 50082-2009.

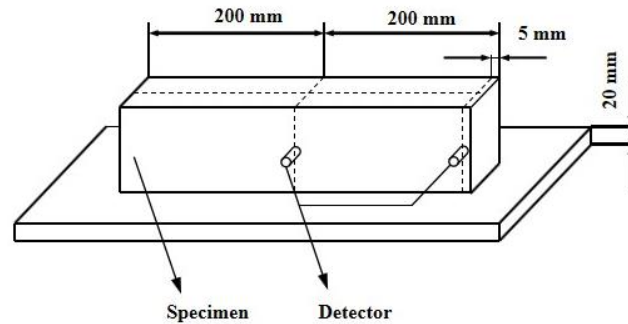


Figure 1. The testing process of the relative dynamic modulus of elasticity.

3. Results and Discussion

3.1. Mechanical Strengths

Figure 2 shows the mechanical strengths (flexural and compressive strengths) of RPC mixed with different dosage of SAC. Table 4 shows the fitting results for the mechanical strengths and the mass ratio (V) of SAC. It can be observed from Figure 2 and Table 4 that the flexural and compressive strengths of RPC at early curing ages (no more than 3 days) increase in the form of a linear function with the mass ratio of SAC. However, when the curing age reaches 7 days, the flexural and compressive strengths decrease linearly with the mass ratio of SAC. This is attributed to the fact that the addition of SAC can effectively improve the early mechanical properties of RPC. Therefore, the flexural and compressive strengths of RPC an early curing age increase with the addition of SAC. However, the mechanical strengths of SAC-based materials are lower than that of ordinary Portland cement when the curing age reaches 7 days [20–22]. Therefore, the flexural and compressive strengths of RPC are reduced by the addition of SAC when the curing age is equal to or higher than 7 days. Finally, the mechanical strengths of RPC cured for equal to or higher than 7 days are obviously higher than that of RPC cured for 1 day and 3 days. Meanwhile, the mechanical strengths of RPC cured for 1 day and 3 days are similar. Additionally, the mechanical strengths of RPC cured for 7 days and 14 days are close to that of specimens cured for 28 days. This is attributed to the fact that the mechanical strengths of RPC with a certain amount of SAC and early strength agent approach the maximum value, therefore, the mechanical strengths of RPC cured for 7 days and 14 days are close to that of specimens cured for 28 days [23–25].

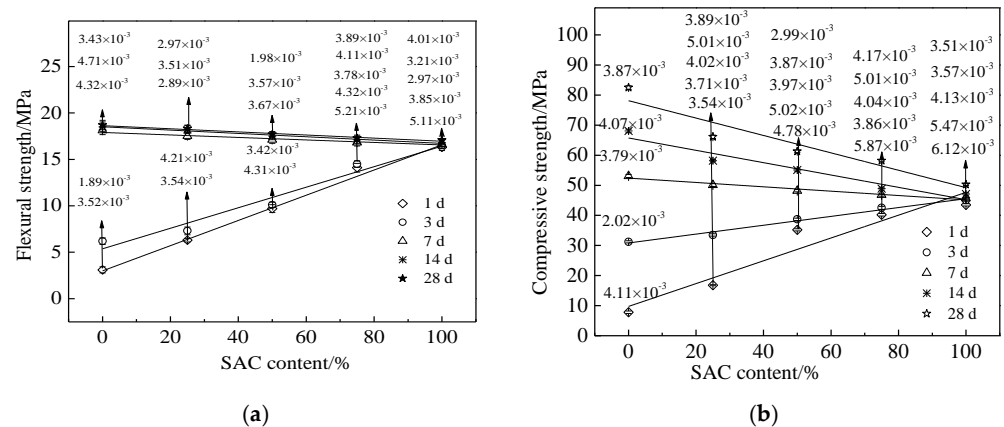


Figure 2. The mechanical strengths of RPC with different dosage of SAC. (a) Flexural strength (f_t), (b) compressive strength (f_{cu}).

Table 4. The fitting results of mechanical strengths and the mass ratio (V) of SAC.

Equation	Curing Time/d	a	b	R^2
$f_t = aV + b$	1	0.136	2.99	0.994
	3	0.111	5.37	0.957
	7	−0.0135	17.90	0.950
	14	−0.0179	18.51	0.967
	28	−0.0168	18.63	0.953
$f_{cu} = aV + b$	1	0.379	9.74	0.900
	3	0.147	30.84	0.980
	7	−0.0724	52.4	0.946
	14	−0.205	65.74	0.918
	28	−0.289	78.14	0.879

Figure 3 shows the relationship between mechanical strengths and the curing time with different dosage of SAC. Table 5 shows the fitting results of the mechanical strengths (flexural strength and compressive strength) and the curing time of RPC with different SAC. It can be observed from Figure 3 that the relationship between mechanical strengths and the curing time conforms to the quadratic function. It can be observed from Table 5 that the fitting degrees of compressive strength are higher than those of flexural strength.

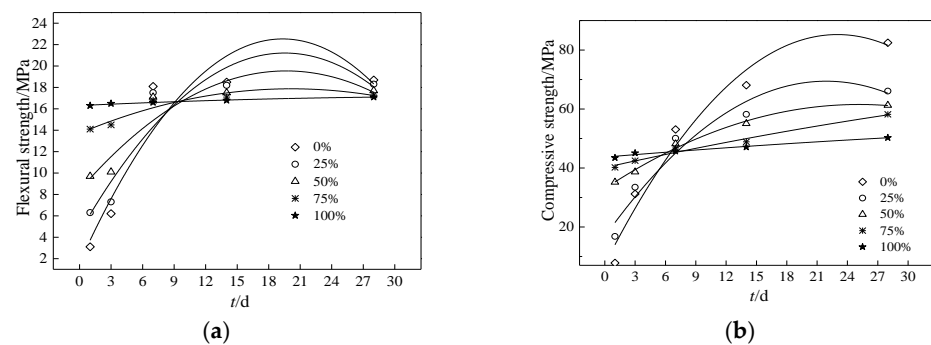
**Figure 3.** The relationship between mechanical strengths and the curing time of RPC with different dosage of SAC. (a) Flexural strength (f_t), (b) compressive strength (f_{cu}).

Figure 4 shows the mechanical strengths (flexural and compressive strengths) of RPC mixed with 50% SAC. Table 6 shows the fitting results of mechanical strengths and the volume ratio (V) of PPFs. The dosage of polypropylene fibers in this study ranges from 0 to 3.5%. As can be observed from Figure 4 and Table 6, the flexural strength firstly increases and then decreases in the form of a quadratic function with the volume of polypropylene fibers. Moreover, as shown in Figure 4, the flexural strength of RPC with 3.0% polypropylene fibers is the highest. However, the compressive strength of RPC increases in the form of quadratic function with the volume of polypropylene fibers. This is attributed to the fact that the polypropylene fibers can bridge the cracks in RPC, thus improving the mechanical properties [26–28]. However, the dispersion efficiency of polypropylene fibers is decreased by the increasing dosage of polypropylene fibers. Therefore, the mechanical strengths remain unchanged after growing to a stable value [29–31].

Table 5. The fitting results of the mechanical strengths (flexural strength and compressive strength) and the curing time (*t*) of RPC with different SAC.

Equation	SAC Content/%	<i>a</i>	<i>b</i>	<i>c</i>	<i>R</i> ²
$f_t = at^2 + bt + c$	0	−0.056	2.165	1.606	0.785
	25	−0.0440	1.717	4.46	0.780
	50	−0.0289	1.135	8.387	0.762
	75	−0.0103	0.413	13.71	0.836
	100	−0.000612	0.0453	16.307	0.962
$f_{cu} = at^2 + bt + c$	0	−0.147	6.772	7.332	0.931
	25	−0.110	4.809	16.780	0.901
	50	−0.0451	2.267	33.035	0.985
	75	−0.00453	0.765	40.149	0.959
	100	−0.00176	0.283	43.702	0.953

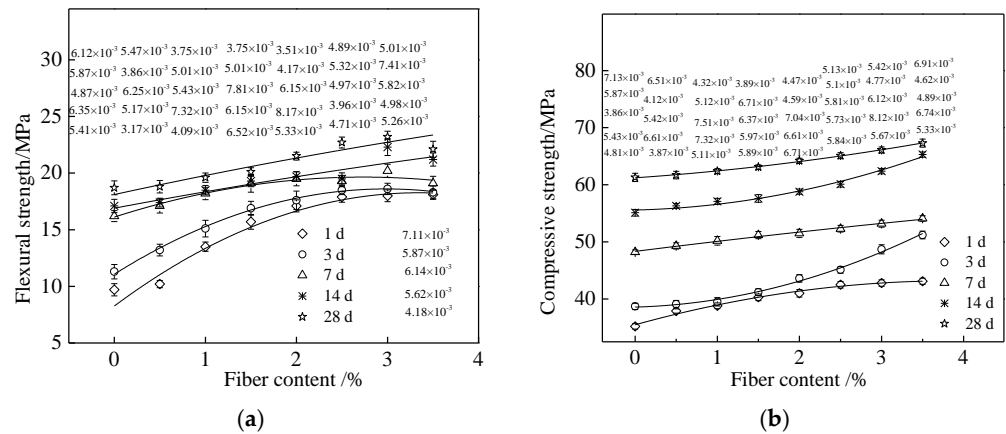


Figure 4. The mechanical strengths of RPC with different dosage of polypropylene fibers. (a) Flexural strength, (b) compressive strength.

Table 6. The fitting results of mechanical strengths and the volume ratio (*V*) of PPFs.

Equation	Curing Age/d	<i>a</i>	<i>b</i>	<i>c</i>	<i>R</i> ²
$f_t = aV^2 + bV + c$	1	−0.895	5.984	8.265	0.952
	3	−0.846	5.047	11.076	0.996
	7	−0.472	2.582	16.119	0.940
	14	−0.0616	1.513	16.904	0.854
	28	−0.0714	1.753	0.847	0.847
$f_{cu} = aV^2 + bV + c$	1	3.981	3.981	35.483	0.983
	3	0.408	0.4081	38.579	0.992
	7	1.805	1.805	48.342	0.988
	14	0.344	0.3441	55.579	0.981
	28	0.993	0.993	61.225	0.998

Figure 5 shows the relationship between the mechanical strengths and the curing time of RPC with different dosage of PPFs. Table 7 presents the fitting results of the mechanical strengths (flexural strength and compressive strength) and the curing time of SAC-RPC with different PPFs. As can be observed from Figure 5, the relationship between mechanical strengths and the curing time fits well with the quadratic function. As can be

observed in Table 7, the compressive strength possesses higher fitting degrees than that of flexural strength.

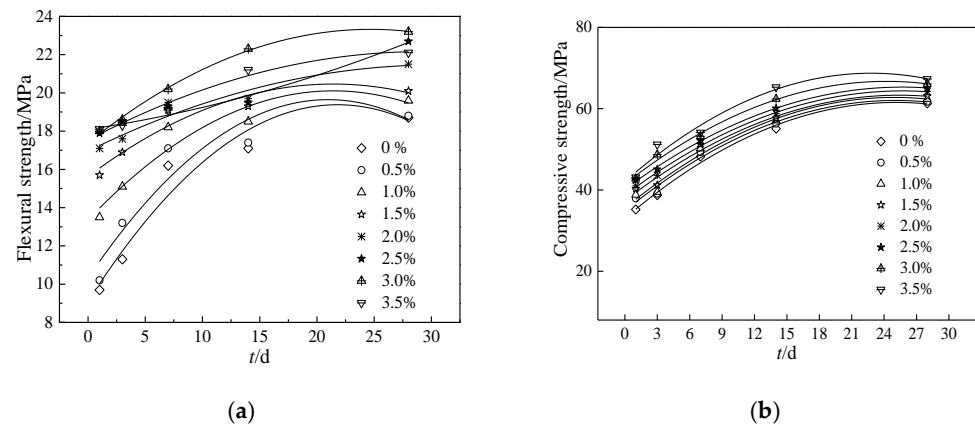


Figure 5. The relationship between the mechanical strengths and the curing time of SAC-RPC with different dosage of PPFs. (a) Flexural strength (f_t), (b) compressive strength (f_{cu}).

Table 7. The fitting results of the mechanical strengths (flexural strength and compressive strength) and the curing time (t) of RPC of different dosage of PPFs.

Equation	PPFs Content/%	a	b	c	R^2
$f_t = at^2 + bt + c$	0	−0.0216	0.943	9.095	0.879
	0.5	−0.0212	0.890	10.317	0.793
	1	−0.0147	0.630	13.357	0.833
	1.5	−0.0106	0.452	15.621	0.827
	2	−0.00484	0.295	16.955	0.877
	2.5	0.00264	0.0885	18.093	0.938
	3	−0.00973	0.481	17.387	0.995
	3.5	−0.00542	0.317	17.528	0.950
$f_{cu} = at^2 + bt + c$	0	−0.0451	2.267	33.035	0.985
	0.5	−0.0432	2.166	34.876	0.970
	1	−0.0438	2.182	35.559	0.961
	1.5	−0.0402	2.041	37.392	0.964
	2	−0.0389	1.997	38.729	0.994
	2.5	−0.0381	1.955	40.205	0.997
	3	−0.0431	2.085	41.489	0.984
	3.5	−0.0512	2.337	42.073	0.942

3.2. Mass Loss of RPC during NaCl Freeze–Thaw Cycles

Figure 6 shows the mass loss of RPC during NaCl freeze–thaw cycles. Table 8 shows the fitting results of mass loss rate and the number of freeze–thaw cycles (N). As depicted in Figure 6 and Table 8, the mass loss ratio increases in the form of a quadratic function. This is attributed to the fact that the frost heave stress can lead to the spalling of RPC specimens [32,33]. Consequently, the mass of RPC decreases with the number of NaCl freeze–thaw cycles. Moreover, as illustrated in Figure 6, the mass loss of RPC is decreased by the increasing dosage of polypropylene fibers due to the fact that the polypropylene fibers can bridge the cracks in RPC during NaCl freeze–thaw cycles, thus preventing the

spalling of concrete [34,35]. Therefore, the polypropylene fibers demonstrate a positive effect on the integrity of RPC, leading eventually to decreasing the mass loss ratio of RPC.

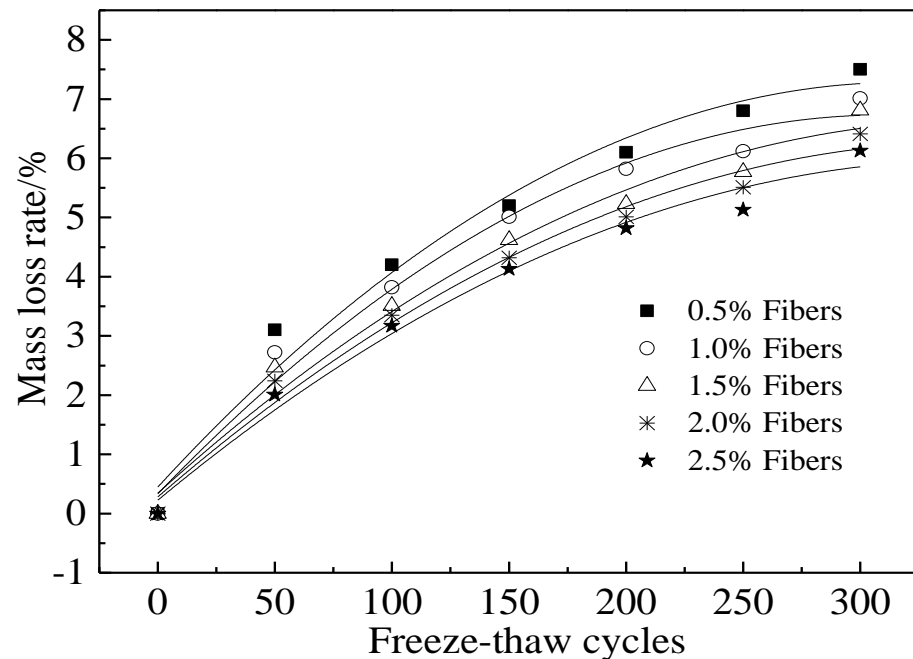


Figure 6. The mass loss of RPC during NaCl freeze–thaw cycles.

Table 8. The fitting results of mass loss rate and the number of freeze–thaw cycles (N).

Equation	PPFs Content/%	a	b	c	R^2
$\frac{\Delta m}{m} = aN^2 + bN + c$	0.5	-6.76×10^{-5}	0.043	0.448	0.968
	1.0	-6.62×10^{-5}	0.0412	0.333	0.975
	1.5	-5.07×10^{-5}	0.0358	0.344	0.971
	2.0	-4.91×10^{-5}	0.0343	0.282	0.979
	2.5	-4.69×10^{-5}	0.0328	0.226	0.979

3.3. Mechanical Strengths Loss Rate of RPC during NaCl Freeze–Thaw Cycles

Figures 7 and 8 show the flexural and compressive strengths loss rate of RPC. Table 9 shows the fitting results of the mechanical strengths loss and the number of freeze–thaw cycles (N). As can be observed from Figures 7 and 8 and Table 9, the flexural strength loss rate increases in the form of a quadratic function, while the compressive strength loss rate increases in the form of linear function. This is attributed to the fact that the NaCl freeze–thaw cycles can lead to the inner damage of RPC [36,37]. Therefore, the mechanical strengths decrease with the number of NaCl freeze–thaw cycles. Meanwhile, the increasing dosage of polypropylene fibers is able to bridge the cracks caused by NaCl freeze–thaw cycles, thus improving the NaCl freeze–thaw resistance and decreasing the mechanical strengths loss of RPC.

Figure 9 shows the relative dynamic elastic modulus ($RDEM$) values of RPC specimens during NaCl freeze–thaw cycles. Table 10 shows the fitting results of the $RDEM$ and the number of freeze–thaw cycles (N). As can be observed from Figure 9 and Table 10, the $RDEM$ decreases in the form of a quadratic function with successive NaCl freeze–thaw cycles. This is attributed to the fact that the NaCl freeze–thaw cycles lead to inner cracks in RPC. The cracks can block the propagation of testing sound waves, thus demonstrating a negative effect on the relative dynamic elastic modulus ($RDEM$) [38].

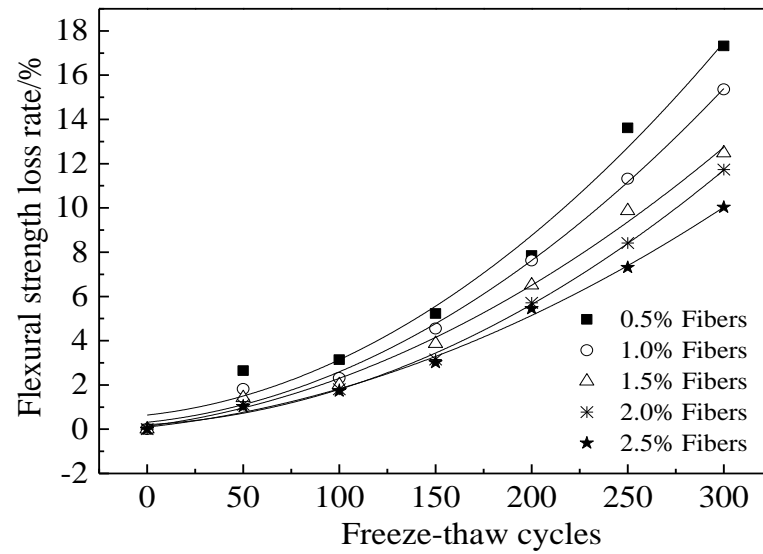


Figure 7. The flexural strength loss rate of RPC during NaCl freeze–thaw cycles.

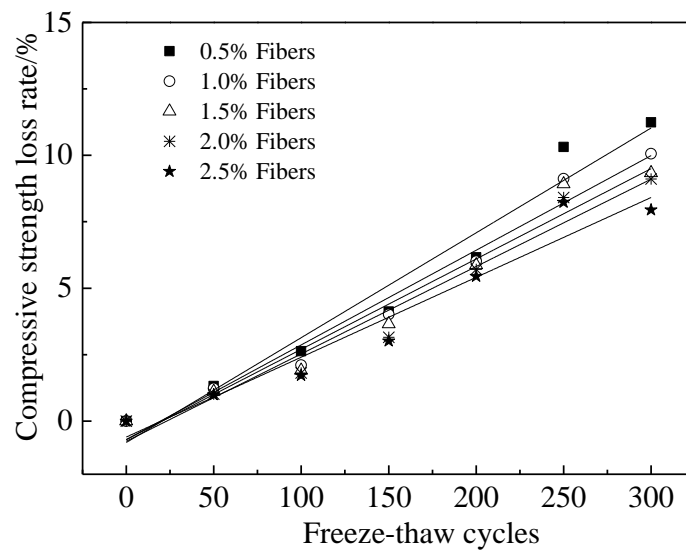


Figure 8. The compressive strength loss rate of RPC during NaCl freeze–thaw cycles.

Table 9. The fitting results of the mechanical strengths loss and the number of freeze–thaw cycles (*N*).

Equation	PPFs Content/%	<i>a</i>	<i>b</i>	<i>c</i>	<i>R</i> ²
$\frac{\Delta f_i}{f_i} = aN^2 + bN + c$	0	1.56×10^{-4}	0.00942	0.640	0.954
	1	1.37×10^{-4}	0.00912	0.313	0.967
	2	1.02×10^{-4}	0.0115	0.133	0.957
	3	1.12×10^{-4}	0.00479	0.206	0.953
	4	7.90×10^{-5}	0.00941	0.0974	0.935
$\frac{\Delta f_{cu}}{f_{cu}} = aN + b$	0	0.0395	−0.806	/	0.983
	1	0.0356	−0.695	/	0.992
	2	0.0340	−0.698	/	0.988
	3	0.0329	−0.759	/	0.981
	4	0.0301	−0.600	/	0.998

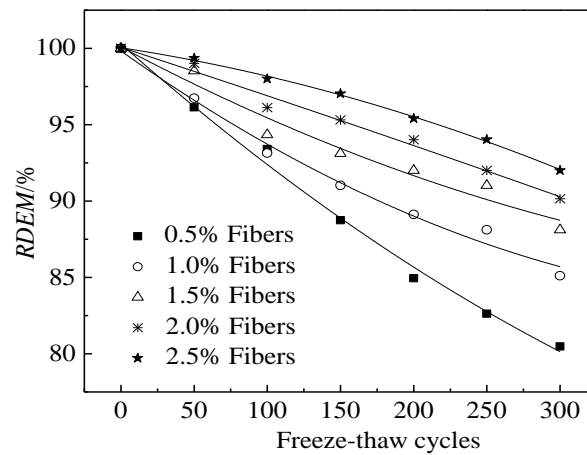


Figure 9. The RDEM during NaCl freeze–thaw cycles.

Table 10. The fitting results of the RDEM and the number of freeze–thaw cycles (N).

Equation	PPFs Content/%	a	b	c	R ²
$RDEM = aN^2 + bN + c$	0	5.90×10^{-5}	-0.08485	100.287	0.992
	1	6.98×10^{-5}	-0.06801	99.827	0.984
	2	4.30×10^{-5}	-0.05075	100.093	0.951
	3	-4.33×10^{-5}	-0.03131	100.070	0.979
	4	-3.97×10^{-5}	-0.01466	100.040	0.997

3.4. Chloride Migration Coefficient during Freeze–Thaw Cycles

Figure 10 shows the chloride migration coefficient (CMC) of RPC during NaCl freeze–thaw cycles. Table 11 shows the fitting results of the CMC and the number of freeze–thaw cycles (N). As can be observed from Figure 8, the chloride migration coefficient of RPC increased in the form of a quadratic function. This is attributed to the fact that the cracks in the RPC increase and widen during NaCl freeze–thaw cycles, thus increasing the NaCl permeability of RPC [39]. The increasing dosage of polypropylene fibers can bridge the cracks in RPC, thus improving the NaCl permeability.

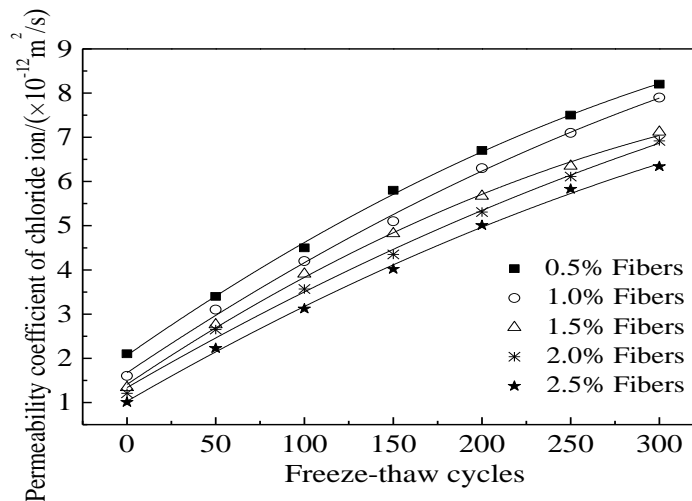


Figure 10. The chloride migration coefficient (CMC) during NaCl freeze–thaw cycles.

Table 11. The fitting results of the CMC and the number of freeze–thaw cycles (N).

Equation	PPFs Content/%	a	b	c	R^2
$CMC = aN^2 + bN + c$	0	-2.52×10^{-5}	0.0281	2.067	0.999
	1	-2.10×10^{-5}	0.0270	1.674	0.997
	2	-2.72×10^{-5}	0.0269	1.411	0.998
	3	-1.61×10^{-5}	0.0233	1.338	0.995
	4	-1.77×10^{-5}	0.0232	1.029	0.998

4. Conclusions

In this study, the mechanical performances and durability of RPC with the assembly unit of sulphoaluminate cement and ordinary Portland cement with polypropylene fibers are investigated. The conclusions are summarized as follows:

The correlation between the mechanical strengths and the mass loss ratio of sulphoaluminate cement follows a linear function and depends on the curing time. Before 7 d of curing, the correlation is positive; however, after 7 d of curing, it changes to negative.

The mechanical strengths exhibit a positive quadratic relationship as a function of polypropylene fiber volume. Specifically, the strengths increase markedly with the increasing dosage of polypropylene fibers and then reach a plateau when the polypropylene fiber volume is over 3.4%.

The mass loss rate and flexural strength loss rate demonstrate a positive quadratic correlation, while the relative dynamic elastic modulus exhibits a negative quadratic function with NaCl freeze–thaw cycles. The compressive strength loss rate increases linearly with freeze–thaw cycles with the addition of polypropylene fibers. With an increase in the fiber contents, the strength loss rate becomes less pronounced, i.e., features an improved freeze–thaw resistance.

Author Contributions: Conceptualization, H.W. and Z.C.; methodology, Z.C.; validation, H.W. and Z.C.; formal analysis, H.W.; investigation, Z.C.; resources, H.W.; data curation, Z.C.; writing—original draft preparation, H.W.; writing—review and editing, H.W.; visualization, Z.C.; supervision, H.W.; project administration, Z.C.; funding acquisition, H.W. All authors have read and agreed to the published version of the manuscript.

Funding: This work is sponsored by the National Natural Science Foundation of China [No. 51808300].

Data Availability Statement: The data used to support the findings of this study are available from the corresponding author upon request.

Conflicts of Interest: The authors declare that there are no conflicts of interest regarding the publication of this paper.

References

- Mo, Z.; Gao, X.; Su, A. Mechanical performances and microstructures of metakaolin contained UHPC matrix under steam curing conditions. *Constr. Build. Mater.* **2021**, *268*, 121112. [[CrossRef](#)]
- Ormellese, M.; Berra, M.; Bolzoni, F.; Pastore, T. Corrosion inhibitors for chlorides induced corrosion in reinforced concrete structures. *Cem. Concr. Res.* **2006**, *36*, 536–547. [[CrossRef](#)]
- Cai, G.; Zhao, J. Application of sulphoaluminate cement to repair deteriorated concrete members in chloride ion rich environment—A basic experimental investigation of durability properties. *KSCE J. Civil Eng.* **2016**, *20*, 2832–2841. [[CrossRef](#)]
- Hong, X.; Wang, H.; Shi, F. Influence of NaCl freeze thaw cycles and cyclic loading on the mechanical performance and permeability of sulphoaluminate cement reactive powder concrete. *Coatings* **2020**, *10*, 1227. [[CrossRef](#)]
- Kuryatnyk, T.; Chabannet, M.; Ambroise, J.; Pera, J. Improvement of calcium sulphate water resistance by addition of calcium sulphoaluminate clinker. *Mater. Lett.* **2008**, *62*, 3713–3715. [[CrossRef](#)]
- Wang, H.; Gao, X.; Liu, J.; Ren, M.; Lu, A. Multi-functional properties of carbon nanofiber reinforced reactive powder concrete. *Constr. Build. Mater.* **2018**, *187*, 699–707. [[CrossRef](#)]

7. Wang, H.; Shi, F.; Shen, J.; Zhang, A.; Zhang, L.; Huang, H.; Liu, J.; Jin, K.; Feng, L.; Tang, Z. Research on the self-sensing and mechanical properties of aligned stainless steel fiber reinforced reactive powder concrete. *Cem. Concr. Compos.* **2021**, *119*, 104001. [[CrossRef](#)]
8. Dong, S.; Han, B.; Yu, X.; Ou, J. Constitutive model and reinforcing mechanisms of uniaxial compressive property for reactive powder concrete with super-fine stainless wire. *Composites Part B* **2019**, *166*, 298–309. [[CrossRef](#)]
9. Dong, S.; Han, B.; Yu, X.; Ou, J. Dynamic impact behavior and constitutive model of super-fine stainless wire reinforced reactive powder concrete. *Construct. Build. Mater.* **2018**, *184*, 602–616. [[CrossRef](#)]
10. Wang, H.; Jin, K.; Zhang, A.; Zhang, L.; Han, Y.; Liu, J.; Shi, F.; Feng, L. External erosion of sodium chloride on the degradation of self-sensing and mechanical properties of aligned stainless steel fiber reinforced reactive powder concrete. *Constr. Build. Mater.* **2021**, *275*, 06629.
11. Wang, H.; Gao, X.; Liu, J. Effects of salt freeze-thaw cycles and cyclic loading on the piezoresistive properties of carbon nanofibers mortar. *Constr. Build. Mater.* **2018**, *177*, 192–201. [[CrossRef](#)]
12. Materazzi, A.; Ubertini, F.; Alessandro, D. Carbon nanotube cement-based transducers for dynamic sensing of strain. *Cement Concr. Compos.* **2013**, *37*, 2–11. [[CrossRef](#)]
13. Dong, S.; Han, B.; Ou, J.; Li, Z.; Han, L.; Yu, X.; Li, Z.; Han, L.; Yu, X. Electrically conductive behaviors and mechanisms of short-cut super-fine stainless wire reinforced reactive powder concrete. *Cement Concr. Compos.* **2016**, *72*, 48–65. [[CrossRef](#)]
14. Gencil, O.; Ozel, C.; Brostow, W.; Martinez-Barrera, G. Mechanical properties of self-compacting concrete reinforced with polypropylene fibres. *Mater. Res. Innov.* **2011**, *15*, 216–225. [[CrossRef](#)]
15. Kakooei, S.; Akil, H.; Jamshidi, M.; Rouhi, J. The effects of polypropylene fibers on the properties of reinforced concrete structures. *Constr. Build. Mater.* **2012**, *27*, 73–77. [[CrossRef](#)]
16. Soutsos, M.; Le, T.; Lampropoulos, A. Flexural performance of fibre reinforced concrete made with steel and synthetic fibres. *Constr. Build. Mater.* **2012**, *36*, 704–710. [[CrossRef](#)]
17. Iyer, P.; Kenno, S.; Das, S. Mechanical properties of fiber-reinforced concrete made with basalt filament fibers. *J. Mater. Civ. Eng.* **2015**, *27*, 04015015. [[CrossRef](#)]
18. *Method of Testing Cements-Determination of Strength*; The State Bureau of Quality and Technical Supervision: Beijing, China, 1999; GB/T 17671-1999.
19. *Standard for Test Method of Long-Term Performance and Durability of Ordinary Concrete*; Ministry of Housing and Urban Rural Development of the People's Republic of China: Beijing, China, 2009.
20. Pelletier-Chaignat, L.; Winnefeld, F.; Lothenbach, B.; Müller, C.J. Beneficial use of limestone filler with calcium sulphoaluminate cement. *Constr. Build. Mater.* **2012**, *26*, 619–627. [[CrossRef](#)]
21. Singh, M.; Kapur, P. Preparation of calcium sulphoaluminate cement using fertiliser plant wastes. *J. Hazard. Mater.* **2008**, *157*, 106–113. [[CrossRef](#)]
22. Velazco, G.; Almanza, J.; Cortés, D.; Escobedo, J.; Escalante-Garcia, J. Effect of citric acid and the hemihydrate amount on the properties of a calcium sulphoaluminate cement. *Mater. Constr.* **2014**, *64*, 1–8. [[CrossRef](#)]
23. Liu, Y.; Tian, W.; Wang, M.; Qi, B.; Wang, W. Rapid strength formation of on-site carbon fiber reinforced high-performance concrete cured by ohmic heating. *Constr. Build. Mater.* **2020**, *244*, 118344. [[CrossRef](#)]
24. Berger, S.; Céline Cau Dit Coumes, J.; Champenois, T.; Douillard, T.; Le Bescop, P.; Aouad, G.; Damidot, D. Stabilization of ZnCl₂-containing wastes using calcium sulfoaluminate cement: Leaching behaviour of the solidified waste form, mechanisms of zinc retention. *J. Hazard. Mater.* **2011**, *194*, 268–276. [[CrossRef](#)] [[PubMed](#)]
25. Aattache, A.; Soltani, R. Durability-related properties of early-age and long-term-resistant laboratory elaborated polymer-based repair mortars. *Constr. Build. Mater.* **2020**, *235*, 117494. [[CrossRef](#)]
26. Ding, Y.; Wang, Q.; Pacheco-Torgal, F.; Zhang, Y. Hybrid effect of basalt fiber textile and macro polypropylene fiber on flexural load-bearing capacity and toughness of two-way concrete slabs. *Constr. Build. Mater.* **2020**, *261*, 119881. [[CrossRef](#)]
27. Li, B.; Chi, Y.; Xu, L.; Shi, Y.; Li, C. Experimental investigation on the flexural behavior of steel-polypropylene hybrid fiber reinforced concrete. *Constr. Build. Mater.* **2018**, *191*, 80–94. [[CrossRef](#)]
28. Shen, D.; Liu, X.; Zeng, X.; Zhao, X.; Jiang, G. Effect of polypropylene plastic fibers length on cracking resistance of high performance concrete at early age. *Constr. Build. Mater.* **2020**, *244*, 117874. [[CrossRef](#)]
29. Shi, F.; Pham, T.; Hao, H. Post-cracking behavior of basalt and macro polypropylene hybrid fibre reinforced concrete with different compressive strengths. *Constr. Build. Mater.* **2020**, *262*, 120108. [[CrossRef](#)]
30. Du, H.X.; Qin, Y.X.; Zhang, W.; Zhang, N.; Hao, X.Y. Mechanics performance of high-performance concrete with polypropylene fibers. *Appl. Mech. Mater.* **2011**, *99–100*, 1233–1238. [[CrossRef](#)]
31. Castoldi, R.; Souza, L.; Andrade Silva, F. Comparative study on the mechanical behavior and durability of polypropylene and sisal fiber reinforced concretes. *Constr. Build. Mater.* **2019**, *211*, 617–628. [[CrossRef](#)]
32. Liu, Q.; Iqbal, M.; Yang, J.; Lu, X.-Y.; Zhang, P.; Rauf, M. Prediction of chloride diffusivity in concrete using artificial neural network: Modelling and performance evaluation. *Constr. Build. Mater.* **2021**, *266*, 12108.
33. Ding, Y.; Huang, Y.; Zhang, Y.; Jalali, S.; Aguiar, J. Self-monitoring of freeze-thaw damage using triphasic electric conductive concrete. *Constr. Build. Mater.* **2015**, *101*, 440–446. [[CrossRef](#)]
34. Wang, Z.; Zeng, Q.; Wang, L.; Yao, Y.; Li, K. Characterizing blended cement pastes under cyclic freeze-thaw actions by electrical resistivity. *Constr. Build. Mater.* **2013**, *44*, 477–486. [[CrossRef](#)]

35. Shi, X.; Fay, L.; Peterson, M. Freeze-thaw damage and chemical change of a portland cement concrete in the presence of diluted deicers. *Mater. Struct.* **2010**, *43*, 933–946. [[CrossRef](#)]
36. Jiang, W.; Shen, X.; Xia, J.; Mao, L.; Yang, J.; Liu, Q. A numerical study on chloride diffusion in freeze-thaw affected concrete. *Constr. Build. Mater.* **2018**, *179*, 553–565. [[CrossRef](#)]
37. Sun, L.; Jiang, K.; Zhu, X.; Xu, L. An alternating experimental study on the combined effect of freeze-thaw and chloride penetration in concrete. *Constr. Build. Mater.* **2020**, *252*, 119025. [[CrossRef](#)]
38. Wang, H.; Gao, X.; Liu, J. Coupling effect of salt freeze-thaw cycles and cyclic loading on performance degradation of carbon nanofiber mortar. *Cold Reg. Sci. Technol.* **2018**, *154*, 95–102. [[CrossRef](#)]
39. Wang, Y.; Liu, Z.; Fu, K. Experimental studies on the chloride ion permeability of concrete considering the effect of freeze–thaw damage. *Constr. Build. Mater.* **2020**, *236*, 117556. [[CrossRef](#)]